Chapter 3

Structure and Phase Behaviour of Binary Mixtures of Cholesterol with DPPC and DMPC

3.1 Introduction

As discussed in chapter 1, phospholipids and cholesterol are important constituents of plasma membranes [1]. The distribution of cholesterol within the membranes is believed to be inhomogeneous and there is some evidence for the existence of cholesterol-rich lipid domains called rafts in these membranes, which are suspected to play a vital role in many cellular events [2, 3, 4, 5]. Although a wide variety of phospholipids are present in cell membranes, the major ones are phosphatidylcholines (PCs). Therefore, PC–cholesterol membranes are excellent model systems to study the effect of cholesterol on lipid membranes.

This chapter deals with x-ray diffraction studies on the structure and phase behaviour of oriented multilayers of dipalmitoyl phosphatidylcholine (DPPC) and dimyristoyl phosphatidylcholine (DMPC) at various cholesterol concentrations. Importance of lipid cholesterol interactions in bio-membranes has led to a large number of studies on these systems. These earlier studies are summarized in section 3.2. We describe our experimental results on DPPC-cholesterol and DMPC-cholesterol mixtures both at high (98 ± 2%) and low (75 ± 2%) relative humidities (RH) in section 3.3. We have used oriented samples in our diffraction experiments which can provide more information about the in-plane ordering and chain tilt. The use of oriented samples has helped us to observe a new modulated phase induced

by cholesterol, which is distinct from the ripple ($P_{\beta'}$) phase observed in pure DPPC and in DPPC–cholesterol mixtures. Structure and electron density map of this phase are presented in section 3.4. A detailed discussion of the structural features and possible origin of the P_{β} phase is given in section 3.5.

3.2 Earlier studies

The importance of lipid-cholesterol membranes has led to a large number of experimental as well as theoretical studies on this system. Spectroscopic studies have been carried out in an attempt to understand the thermotropic phase behaviour of phospholipid-cholesterol mixtures [6, 7, 8, 9, 10, 11, 12, 13, 14, 15]. Differential scanning calorimetry (DSC) studies show a progressive decrease in the temperatures associated with main transition (T_m) and pre-transition (T_p) , and in the corresponding transition enthalpies with increasing cholesterol concentration (X_c). In these studies, the pre-transition was observed up to $\sim$ 7 mol% of cholesterol, whereas the main transition completely disappears at $X_c > 50$ mol% [11, 12].

The phase behaviour, degree of ordering of the hydrocarbon chains, and lateral diffusion in the presence of cholesterol have been probed by nuclear magnetic resonance (NMR) [7, 8]. Phase diagram obtained from the NMR study by Vist et al. is shown in Fig. 3.1. A cholesterol–rich β phase was found to coexist with both L_{α} and $L_{\beta'}$ phases over a wide cholesterol concentration range at temperatures above and below the main transition, respectively. Degree of ordering of the hydrocarbon chains and the in-plane diffusion rates in this phase were found to be intermediate between those in the fluid (L_{α}) and gel ($L_{\beta'}$) phases. At higher cholesterol concentrations (> 20 mol%) the β phase exists throughout the temperature range as shown in the phase diagram. The β and L_{α} phases are often referred to as the liquid ordered (l_o) and liquid disordered (l_d) phases, respectively, in the literature [14, 16, 17]. The l_o phase is believed to be rich in cholesterol, whereas the l_d phase is poor in cholesterol. Hydrocarbon chain segmental order parameter in the l_o phase is found to be almost twice compared to that in the pure lipid at temperatures above the chain melting transition [8].

The two-phase region above the main transition observed in NMR studies has not been

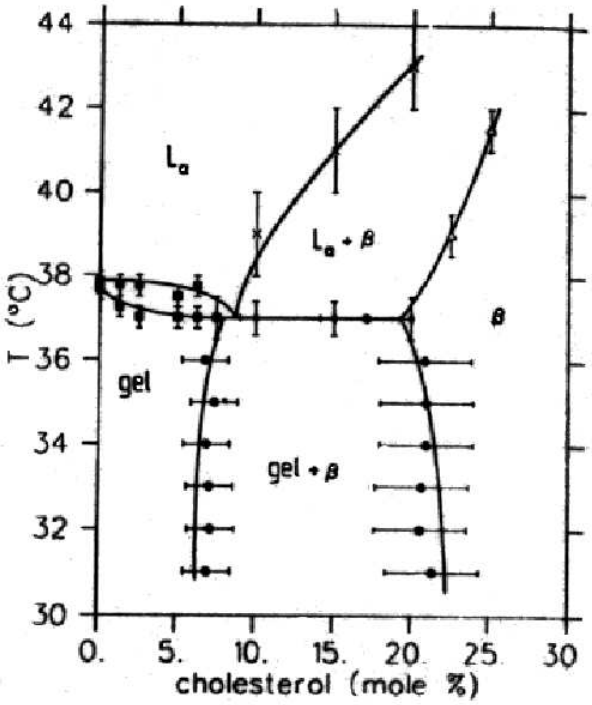

Figure 3.1: Phase diagram of DPPC–cholesterol mixtures obtained from NMR studies [7]. β is the cholesterol–rich phase.

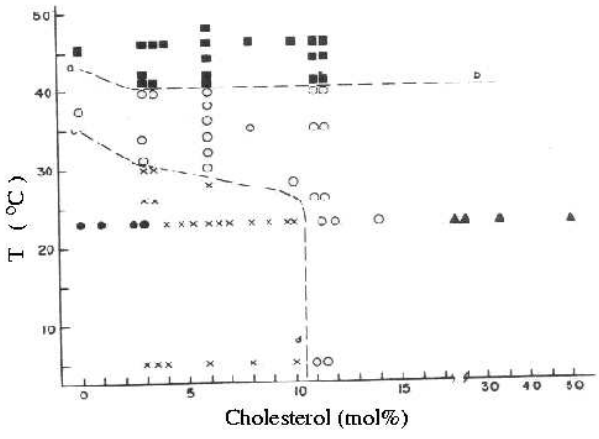

Figure 3.2: Phase diagram of DPPC–cholesterol mixtures obtained from x-ray diffraction studies [18]. "×" corresponds to two-phase region of two lamellar phases and all other symbols represent single lamellar phase.

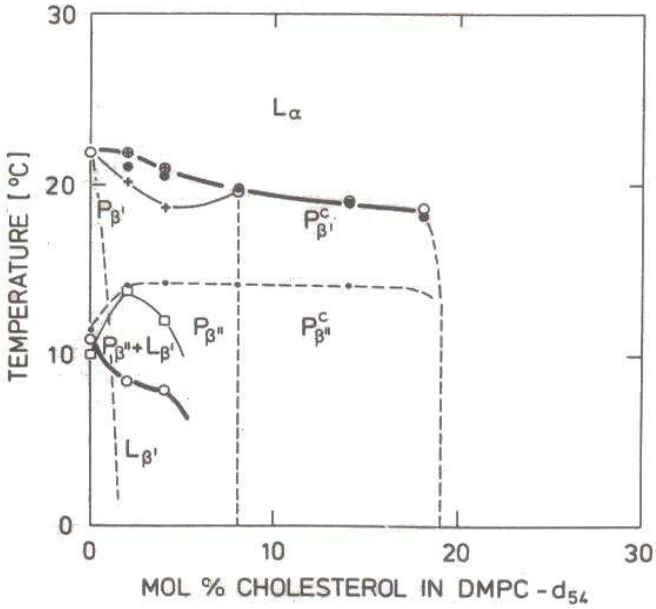

Figure 3.3: Phase diagram of DMPC–cholesterol mixtures obtained from neutron scattering studies [19]. As discussed in the text the dependence of λ on X_c is different for temperatures $> 15°C$ and $< 15°C$. This difference is indicated by the symbols $P_{\beta'}$ and $P_{\beta''}$. The superscript c stands for cholesterol.

seen in diffraction experiments [18, 19, 20]. However, these studies have found two-phase coexistence below the main transition at $X_c < 10$ mol%. One of these two phases, which is presumably richer in cholesterol can swell more and has a lamellar spacing d ~ 80 Å [18]. This phase persists even at higher cholesterol concentrations, whereas the cholesterol–poor phase disappears above 10 mol% (Fig. 3.2). The d-spacing of this phase is ~ 67 Å.

The ripple phase in DMPC–cholesterol mixtures has been observed up to $X_c = 20$ mol% in both small angle neutron scattering (SANS) and freeze fracture studies [19, 21]. The phase diagram determined from the SANS study is shown in Fig. 3.3. These studies also found a secondary ripple for $X_c < 5$ mol% which has a wavelength 1.9 times larger than the primary ripple (Fig. 3.4 a). The secondary ripple wavelength was found to decrease with increasing temperature. No secondary ripple was observed above 5 mol% (Fig. 3.4 b). In SANS studies the wavelength (λ) of the ripple at higher temperatures ($> 15°C$) increases gradually with X_c. λ increases with X_c from ~ 150 Å at 0 mol% to ~ 500 Å at 20 mol%. Similar behaviour was found for the primary ripple in freeze fracture study. However, at lower temperatures, λ stays relatively constant at ~ 250 Å till $X_c \approx 8$ mol%, and then increases as at higher temperatures.

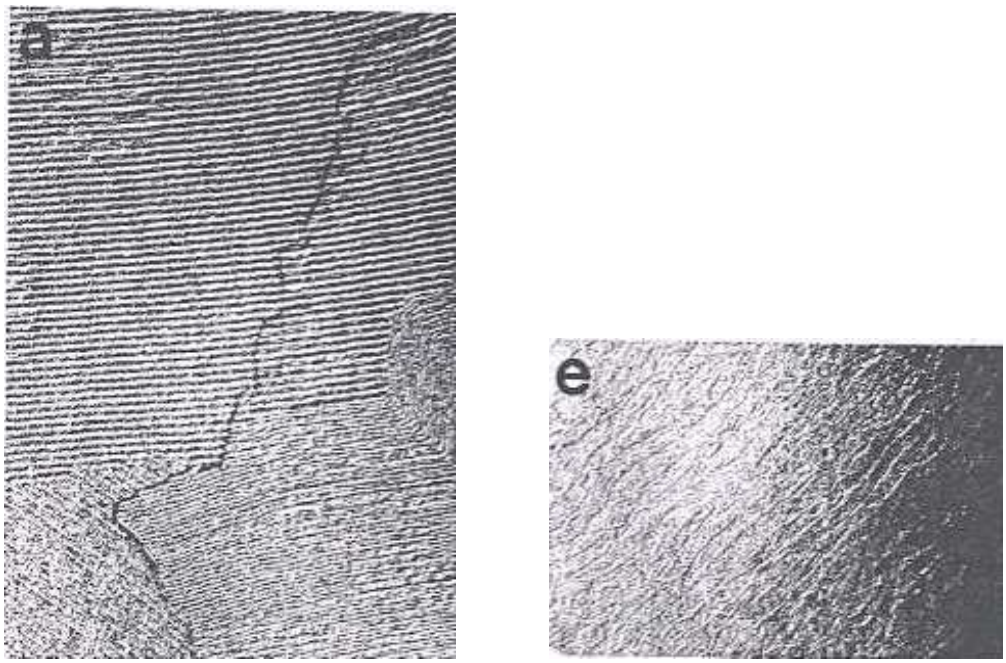

(a) (b)

Figure 3.4: Freeze-fracture electron micrographs of the ripple structure of pure DMPC (a) and mixture of DMPC with 16 mol% cholesterol (b). (a) shows both the primary and secondary ripple structure [21].

Therefore, the dependence of λ with X_c is different for higher and lower temperatures. This difference is indicated by the symbols $P_{\beta'}$ and $P_{\beta''}$ in Fig. 3.3. No ripples were observed for $X_c > 20$ mol%.

The variation of λ with X_c in the range $0 \leq X_c < 20$ was found to be described by $\frac{d}{d_0} = \frac{0.2}{0.2-X_c}$ [21], where d and d_o are the wavelength of ripples with and without cholesterol, respectively (Fig. 3.5 a). d is found to diverge at $X_c = 20$ mol%. The proposed model used to calculate the relation between X_c and $\frac{d}{d_0}$ is shown in Fig. 3.5 b. For $X_c < 20$ mol%, the model was based on ordered microscopic phase separation between strips of width d_0 corresponding to pure DMPC and strips of width d_{20} corresponding to $X_c = 20$ mol% (Fig. 3.5 b). The amplitude of the ripple did not seem to change with X_c. A similar trend has been observed in SANS study on mixtures of cholesterol with DMPC with deuterated hydrocarbon chains [19]. In these studies, λ was found to be strongly temperature dependent. λ decreases first with increasing temperature and then increases slightly near the main transition at a given X_c [19]. No macroscopic domains of two different ripples were observed in these studies other

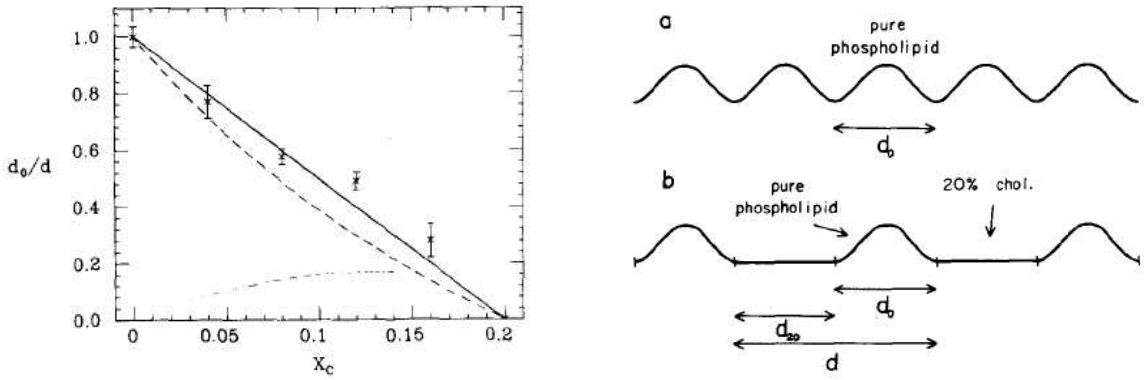

(a) (b)

Figure 3.5: Variation of ripple wavelength (d) with cholesterol compositions (X_c) (a). d_0 is the ripple repeat distance corresponding to pure DMPC. The points and the solid line was obtained from experiments, whereas, the dotted line was determined from the model shown in (b) [21].

than the primary and secondary ripples found at $X_c < 5$ mol%.

Time resolved small angle x-ray diffraction studies on DMPC–cholesterol mixtures have indicated phase separation at higher temperatures (> 50°C) for $10 < X_c < 20$, which is believed to arise from two different arrangements of cholesterol molecules in the bilayer [22]. However, no phase separation between two fluid phases has ever been observed in any of the diffraction experiments at lower temperatures.

3.3 Experimental results

Small angle scattering techniques can in principle detect microscopic phase separation in the plane of bilayers, if there is sufficient contrast in the scattering densities of the two phases. However, even in the absence of such contrast, macroscopic phase separation can easily be detected from non-overlapping reflections in the diffraction pattern coming from the individual phases. On the basis of the diffraction patterns we have determined partial phase diagrams of the two binary systems.

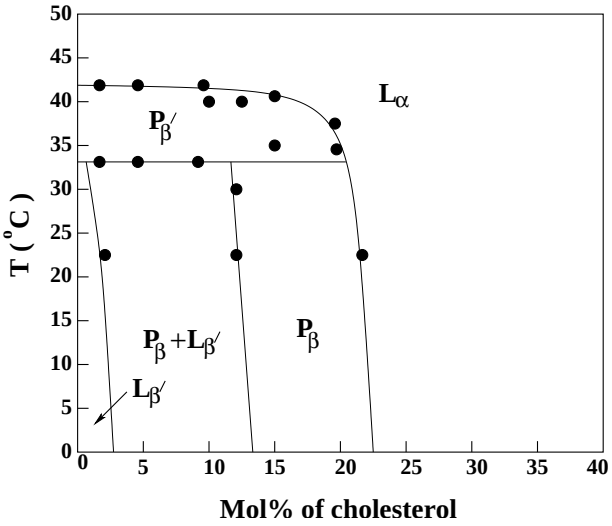

Figure 3.6: Phase diagram of DPPC–cholesterol mixtures at 98% RH, determined from diffraction data. Data points correspond to temperatures where a change in diffraction pattern was observed. In the coexistence regions the superposition of two diffraction patterns was observed.

3.3.1 DPPC–cholesterol at 98 ± 2% relative humidity (RH)

DPPC exhibits three lamellar phases at high hydration, consisting of stacks of bilayers separated by water; the fluid (L_α) phase above the main transition, the gel ($L_{\beta'}$) phase below the pre-transition and the ripple ($P_{\beta'}$) phase in between. Diffraction patterns of pure DPPC obtained by us are consistent with a main transition at ~ 42°C and a pre transition at ~ 34°C, in agreement with earlier studies [23]. In the gel phase of DPPC, we see two wide angle reflections, one on-axis ($q_z = 0$) and the other off-axis ($q_z \neq 0$) coming from the quasi-hexagonal lattice of hydrocarbon chains of lipid molecules. As discussed in chapter 2, the wide angle spot at $q_z \neq 0$ indicates that the molecules are tilted with respect to the bilayer normal and that the direction of the tilt is towards nearest neighbour. Tilt angle measured from the position of the wide angle reflection is 30° [24].

Phase diagram of DPPC–cholesterol mixtures at 98% RH has been constructed from the diffraction data and is presented in Fig. 3.6. The gel ($L_{\beta'}$) phase was identified from the presence of sharp chain reflections in the wide angle region of the diffraction pattern [25], whereas the modulated (P_β) phase was identified from the presence of "satellite" reflections in the small angle region (Fig. 3.7 a). The latter phase is characterized by a rectangular unit

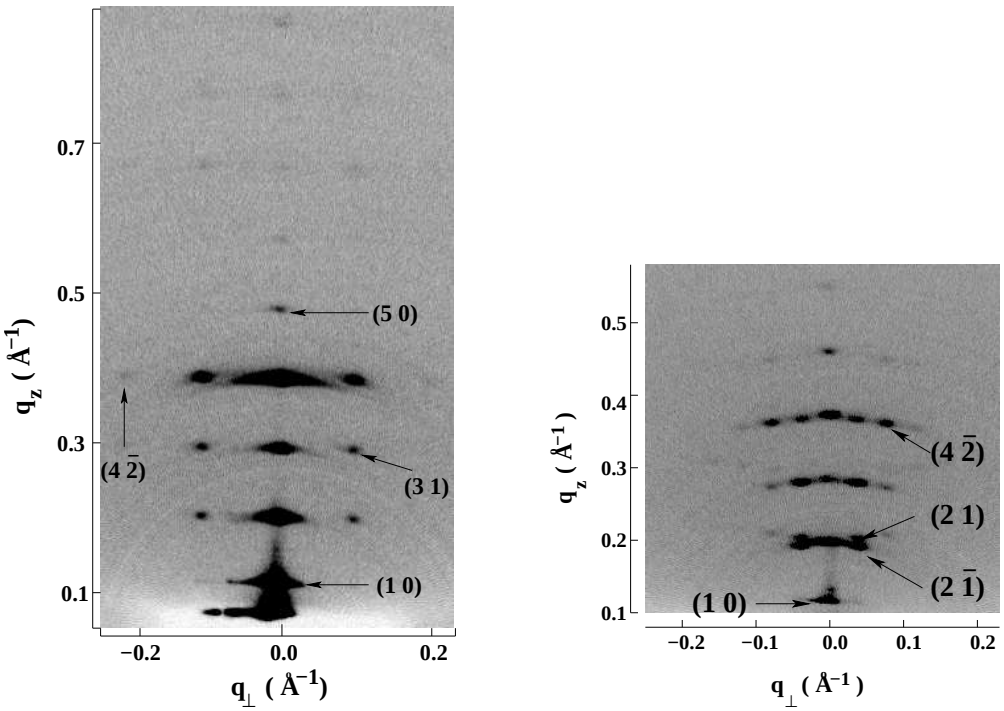

(a) (b)

Figure 3.7: (a) Diffraction pattern of the P_β phase of DPPC–cholesterol mixtures at 98 % RH (X_c = 15 mol%, T = 6°C). The reflections can be indexed on a primitive rectangular lattice as shown (d = 66.3 Å, λ = 60.7 Å). For comparison the diffraction pattern of the ripple ($P_{\beta'}$) phase of DMPC (T = 20°C, RH =98%), that occurs in between the pre- and main-transitions is shown in (b) (d = 57.6 Å, λ = 158 Å). These reflection can be indexed on an oblique lattice as shown.

cell, unlike the usual ripple ($P_{\beta'}$) phase, occurring in between the pre- and main-transitions, which has an oblique unit cell (Fig. 3.7 b). Incorporation of 2.5 to 10 mol% cholesterol does not affect the main- and pre-transition temperatures significantly. The diffraction pattern of the ripple phase suggests an increase in the wavelength with cholesterol content, as found in earlier studies [6, 21]. For 2.5 < X_c < 12.5, below pretransition we observe two sets of reflections in the small angle region, indicating the coexistence of the gel and P_β phases (Fig. 3.8). The coexistence of these two phases persists even at lower temperatures down to 5°C. Tilt angle of the gel phase remains the same as that in pure DPPC. At X_c = 12.5 mol%, the P_β phase appears at ~ 31°C and continues down to 25°C. Below 25°C it coexists with $L_{\beta'}$.

For 15 < X_c < 20, pre-transition disappears and the P_β phase exists down to the lowest temperature studied (5°C). The wide angle reflections at q_z = 0 in the P_β phase indicates that

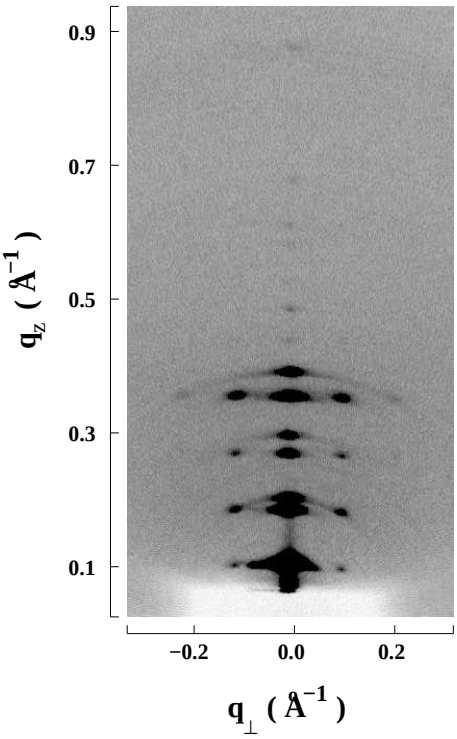

Figure 3.8: Diffraction pattern showing the coexistence of the gel and P_β phases (X_c = 10 mol%, T= 10 °C, RH = 98 %).

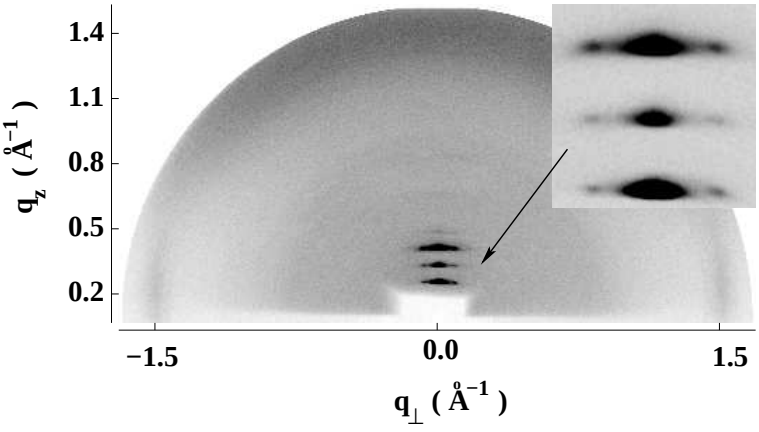

Figure 3.9: Diffraction pattern of the P_β phase. Inset shows the small angle region of the diffraction pattern on an expanded scale and at a higher contrast (X_c = 12.5 mol%, T= 24 °C, RH = 98 %). Note the wide angle reflections at $q_z \simeq 0$.

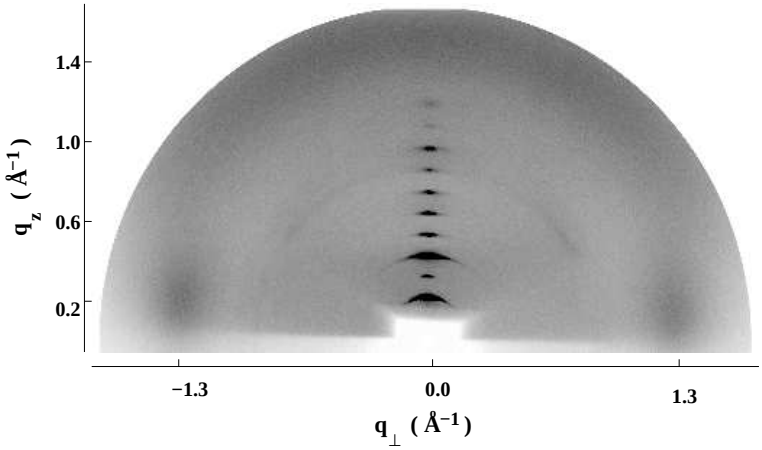

Figure 3.10: Diffraction pattern of the cholesterol–rich l_o phase (X_c = 50 mol%, T= 55°C, RH = 98 %). The first order lamellar peak is masked by the beam stop. Note that the wide angle chain reflections are condensed along q_z.

the average chain tilt with respect to the bilayer normal is zero (Fig. 3.9). Increasing X_c further leads to a fluid phase, often called the liquid ordered (l_o) phase in the literature . As can be seen from Fig. 3.10, the wide angle chain reflections get condensed along q_z in the presence of cholesterol. In addition the spacing of these reflections also change with X_c. For example, it changes from 4.2 Å to 4.9 Å as X_c is increased from 20 to 55 mol% at 25 °C (Fig. 3.11). The phase boundary between l_o and P_β is detected at X_c = 22 mol%.

For $X_c \geq 50$ mol%, we obtain diffraction patterns with a large number of sharp reflections on initial heating of the sample (Fig. 3.12) [26]. This structure melts into the l_o phase at ~ 50°C on heating and is not seen on cooling down to 5°C. This structure was not probed in any detail in the present study. The diffraction data at 98% RH are summarized in table 3.1. The dependence of λ with temperature at X_c = 12.5 mol% and its variation with X_c at T = 15°C are shown in Fig. 3.13 a and b, respectively. λ increases with temperature and decreases with X_c.

Unoriented samples of a few binary mixtures of DPPC and cholesterol were studied in order to investigate their behaviour in excess water. d-spacing in the L_α phase of pure DPPC was found to be 65 Å, whereas it decreases to 63.4 Å in the gel phase. At X_c = 5 and 10 mol%, the typical range of X_c in which the P_β phase occurs, the d-spacing increases drastically to 74.5 Å and 85.7 Å, respectively, at T = 25°C. However, at these X_c there is a sudden jump in

Table 3.1: Lamellar spacings d (Å) of DPPC-cholesterol mixtures as a function of temperature. Two sets of spacings indicate the coexistence of the $L_{\beta'}$ and P_β phases. Numbers in brackets correspond to the wavelength of the P_β or the $P_{\beta'}$ phase. $*$ and † denote the ripple ($P_{\beta'}$) and P_β phases, respectively, which were identified from the smearing of the lamellar reflections. RH = 98 ±2 %. The error in d is ± 0.3 Å .

T (°C)	X_c (mol%)					
	0	5	10	12.5	15	20
45	56.6	-	59.1	59.8	59.2	59.2
40	62.3 (145)	61.5*	62.9*	61.8*	63.5	62.6
35	60.3*	61.0*	62.9*	64.7†	65.4 (79.5)	63.9†
30	60.0	59.2 ; 61.5†	61.4 ; 66.0 (84.9)	65.4 (76.0)	65.7 (79.5)	63.9 (74.0)
25	59.7	59.5 ; 64.0 (75.8)	62.0 ; 67.4 (77.7)	66.5 (74.0)	65.7 (66.8)	63.9 (63.2)
20	63.9	59.5 ; 64.0 (70.6)	60.8 ; 66.8 (75.5)	60.5 ; 66.9 (69.5)	67.0 (66.8)	67.4 (60.7)
15	62.0	59.7 ; 64.6 (68.9)	60.3 ; 66.8 (69.3)	59.9 ; 66.3 (65.4)	66.7 (63.0)	67.4 (60.7)
10	62.0	59.7 ; 64.6 (68.9)	60.3 ; 66.5 (67.9)	59.9 ; 66.9 (65.4)	66.7 (63.0)	67.4 (58.3)
5	-	-	60.3 ; 66.5 (66.6)	59.9 ; 66.3 (62.3)	66.3 (60.7)	-
	22	33	40	45	50	55
45	60.6	60.7	61.0	59.7	59.1	57.9
40	63.1	60.7	61.0	59.7	59.5	57.7
35	63.8	60.7	61.0	59.7	58.5	57.5
30	63.8	60.7	61.0	59.4	58.4	57.3
25	63.8	60.7	62.1	60.5	58.8	58.3
20	65.3	60.7	62.1	60.8	59.5	58.1
15	65.3	60.7	61.9	60.4	59.4	58.0
10	65.3 (51.2)	60.7	61.3	60.2	59.3	57.8
5	65.3 (51.2)	-	61.6	59.9	58.2	57.3

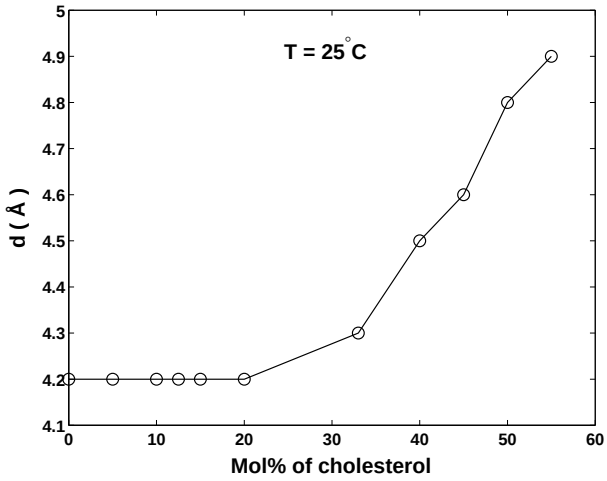

Figure 3.11: Variation of d-spacing of the wide angle reflection with cholesterol concentration (T= 25°C, RH = 98 %).

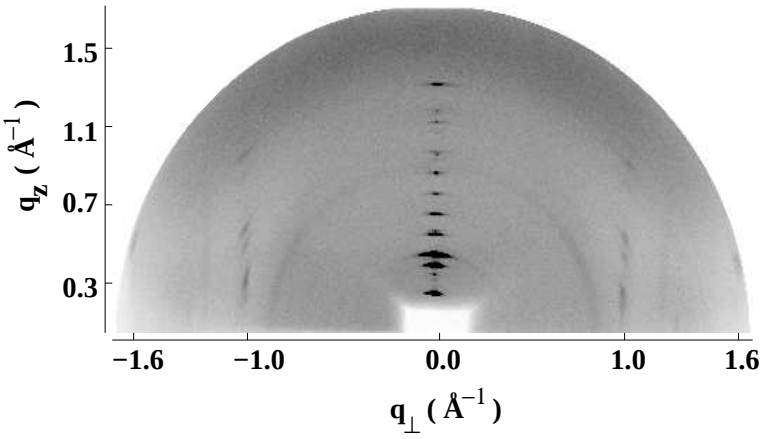

Figure 3.12: Diffraction pattern of a highly ordered phase of DPPC at X_c = 55 mol% before heating the sample to high temperature.

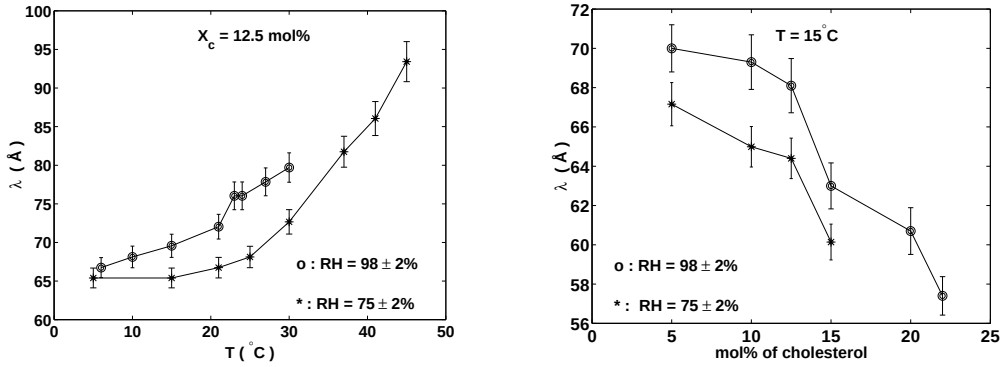

(a) (b)

Figure 3.13: Variation of the wavelength of modulation (λ) of the P_β phase of DPPC-cholesterol mixtures with temperature at X_c = 12.5 mol% (a) and with X_c at T = 15°C. (b).

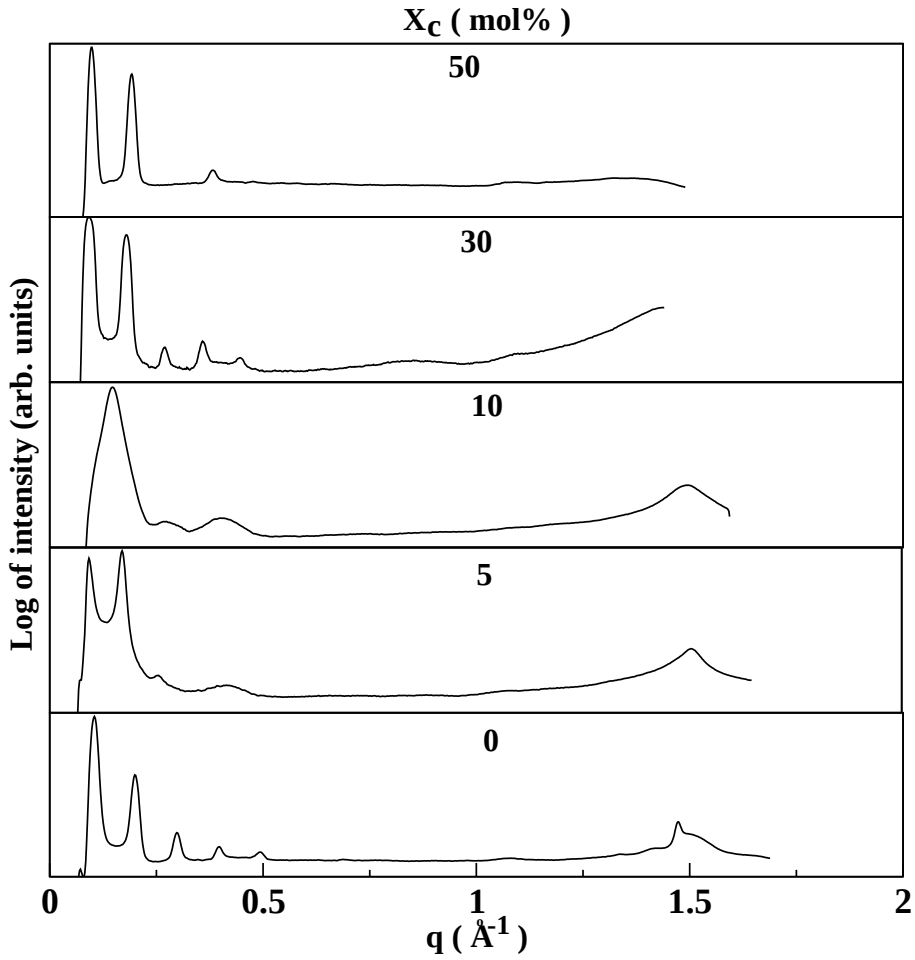

Figure 3.14: Plot of intensity vs. q obtained from unoriented samples of DPPC-cholesterol mixtures with excess water at 25°C.

the d-spacing at T_m, indicating the phase transition from P_β to L_α phase. At X_c = 33 and 50 mol%, there is no change in the d-spacing with increasing temperature, indicating a single cholesterol–rich fluid (l_o) phase. Plots of intensity vs. q for different X_c are shown in Fig. 3.14. As seen in Fig. 3.14, the position of the wide angle reflection is shifted towards lower q value at higher X_c as found in case of aligned samples. The widths of the wide angle profiles get broadened on incresing X_c, as in aligned samples. The d-spacings obtained at 25°C and 50°C are given in table 3.2. In these mixtures, we have not observed any macroscopic phase separation.

It has been reported in the literature that the cholesterol–rich l_o phase is insoluble in aqueous solution of non ionic detergents like Triton X-100 at 4°C[27]. This detergent insoluble fraction is known as detergent resistant membranes (DRM). However, it was not very clear

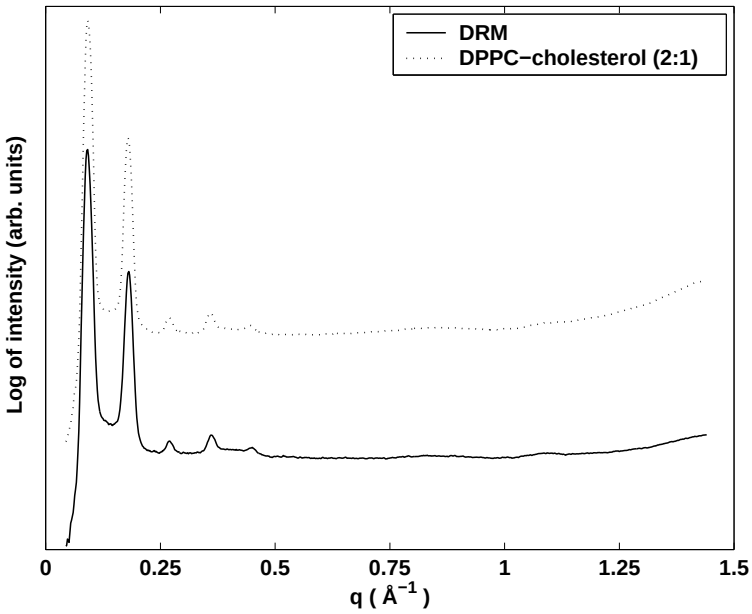

Figure 3.15: Plot of intensity vs. q of the l_o phase ($\cdots$) and of the detergent resistant membranes (DRM) (—). DRM form after adding Triton X-100 to the l_o phase at 4°C. (X_c = 33 mol%, T= 25°C).

Table 3.2: Lamellar spacings d (Å) obtained from unoriented samples of DPPC-cholesterol mixtures in excess water. The error in d is ± 0.9 Å.

T (°C)	X_c (mol%)				
	0	5	10	33	50
25	63.4	74.5	85.7	68.9	65.8
50	65.0	65.4	67.8	–	65.2

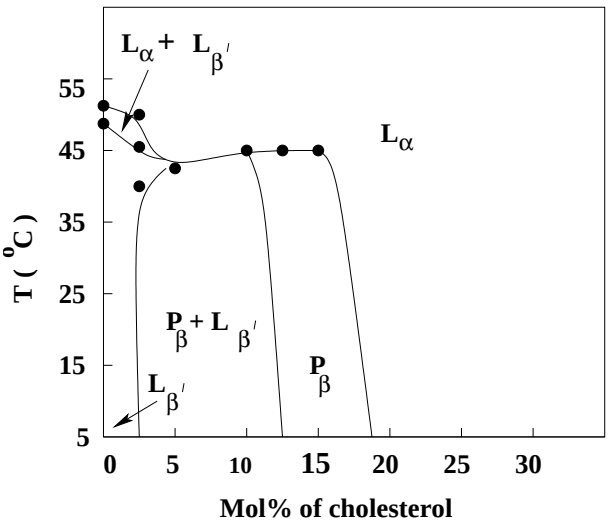

Figure 3.16: Phase diagram of DPPC–cholesterol mixtures at 75 ±2% RH, determined from the diffraction data.

if the DRM has the same composition as the l_o phase. In order to check this possibility we have done the experiments with l_o phase of DPPC-cholesterol mixture at X_c = 33 mol% and the DRM obtained from it by adding 1 ml of 1% Triton X-100 at 4°C. We have observed identical diffraction patterns from these two systems, as shown in the Fig. 3.15, suggesting that DRM has the same composition as the l_o phase.

3.3.2 DPPC–cholesterol at 75% RH

The phase behaviour of DPPC–cholesterol mixtures has also been examined at 75 ± 2% RH (Fig. 3.16). The main transition temperature (T_m) of pure DPPC increases to 50°C and pre-transition disappears and hence the $P_{\beta'}$ phase was found to be absent, in agreement with earlier studies [25]. A small coexistence region of L_α and $L_{\beta'}$ has been detected from the diffraction pattern at $X_c < 5$ mol%. Such a coexistence in the pure lipid is unexpected since by fixing the RH what we have is essentially a single component system. Presently we do not know the origin of this discrepancy. For $2.5 < X_c < 12.5$, the coexistence of the gel and P_β phases has been identified from their characteristic diffraction patterns, as discussed in the previous section. The P_β phase is stabilized at this lower RH and occurs over a wider range of temperature from 45°C to 5°C (Fig. 3.17). Wide angle reflection seen at $q_z = 0$ indicates the absence of an average chain tilt in this phase as found at 98% RH. The range of

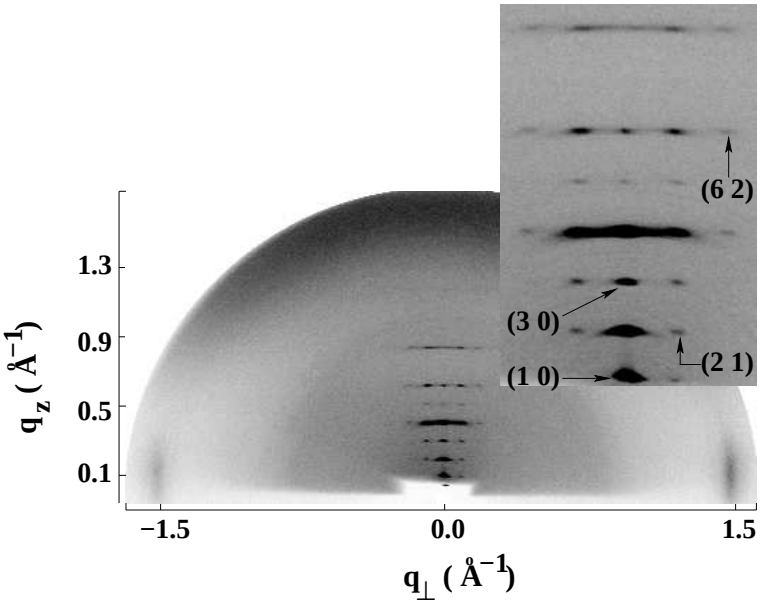

Figure 3.17: Diffraction pattern of DPPC at X_c = 12.5 mol% (T = 21°C, RH =75 ± 2%) The inset shows the small angle region of the diffraction pattern on an expanded scale. The reflections are indexed on a primitive rectangular lattice as shown.

X_c over which it was found is very similar to that at 98% RH, although the P_β - l_o boundary is shifted to a slightly lower value of X_c. The wavelength of modulation (λ) of the P_β phase was found to vary both with temperature and X_c, as shown in Fig. 3.13. At 5°C, $\lambda \sim 65$ Å both at 98% and 75% RH. λ decreases with X_c, with the rate of decrease increasing considerably on approaching the P_β - l_o phase boundary. The d-spacings obtained from the experiments at 75% RH are summarized in table 3.3

3.3.3 DPPC–dehydroergosterol (DHE)

The sterol DHE has been often used as a cholesterol analog in many studies. We have studied a DPPC–DHE mixture in order to check the influence of sterol structure on the modulated phase. The structure of DHE is similar to that of cholesterol except for the presence of three additional double bonds, and an extra CH_3 group in the hydrocarbon chain. We have only studied one composition of DHE (13 mol%) with DPPC at both 98% and 75% RH. Near the main transtion the L_α and $P_{\beta'}$ phases were found to coexist over a narrow temperature range at both these relative humidities. At lower temperatures, the $P_{\beta'}$ phase was found throughout the temperature range studied (Fig. 3.18). However, we have observed additional reflections

Table 3.3: Lamellar spacings d (Å) of DPPC-cholesterol mixtures as a function of temperature. Two sets of spacings indicate the coexistence of the $L_{\beta'}$ and P_β phases. Numbers in brackets correspond to the wavelength of the P_β phase. RH = 75 ±2 %. The error in d is ± 0.3 Å .

T (°C)	X_c (mol%)						
	0	2.5	5	10	12.5	15	20
55	51.1	51.2	52.6	53.5	53.7	54.2	54.7
50	51.2 ; 55.4	51.3 ; 54.7	52.0	55.8	-	56.1	56.0
45	55.4	56.1	55.1	55.6 ; 57.6 (104.0)	58.8 (93.4)	58.2	57.2
40	55.5	57.6 ; 56.1	56.3 ; 57.8	55.6 ; 58.0 (84.0)	59.2 (81.0)	58.6 (81.1)	57.2
35	55.5	58.6 ; 56.1	56.4 ; 58.4	55.6 ; 58.6 (81.0)	59.6 (79.8)	-	58.4
30	55.8	57.8 ; 56.1	-	55.6 ; 58.8 (75.0)	60.7 (68.1)	59.3 (72.5)	58.4
25	55.8	58.6 ; 56.1	56.4 ; 58.8	56.0 ; 59.3 (73.8)	61.0 (68.1)	59.9 (66.5)	59.2
20	55.8	59.3 ; 56.5	56.4 ; 58.9	56.0 ; 59.7 (68.8)	61.4 (67.5)	59.9 (62.4)	59.2
15	55.8	59.3 ; 56.5	56.5 ; 59.2	56.0 ; 59.7 (65.5)	61.8 (64.5)	-	-
10	55.8	59.3 ; 56.4	56.5 ; 59.2	56.0 ; 59.7 (65.5)	62.0 (64.2)	60.3 (60.6)	59.8
5	55.8	59.5 ; 56.1	56.3 ; 59.7	56.0 ; 59.7 (64.4)	62.0 (64.2)	-	-

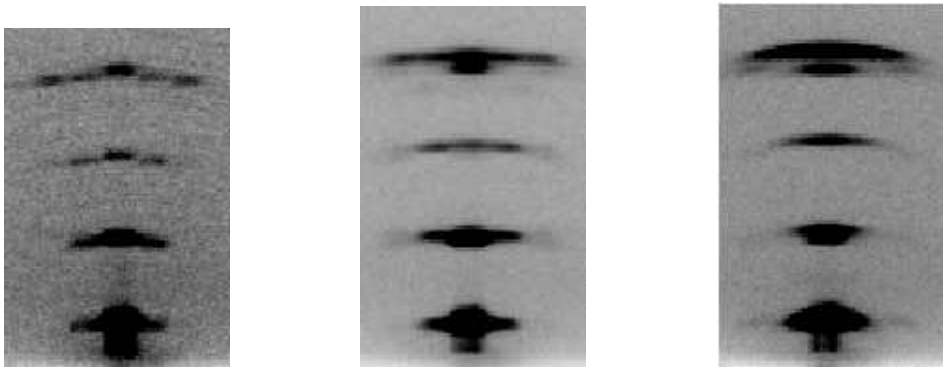

(a) (62.4) (b) (63.7 ; 65.7) (c) (59.3 ; 62.7)

Figure 3.18: Small angle region of diffraction patterns of DPPC-DHE mixtures (X_c = 13 mol%) showing $P_{\beta'}$ phase of wavelength ~ 150 Å(T = 35°C, RH = 98%)(a) and the coexistence of the $P_{\beta'}$ phase with the P_β (T = 10°C, RH = 98%) (b). (c) is same as (b) but obtained at 75% RH. The wavelength of the P_β is ~ 70 Å. Numbers in brackets represent d-spacing (Å) corresponding to the reflections.

Table 3.4: Spacings d (Å) of DPPC with 13 mol% of DHE obtained at two different RH and at different temperatures. Two sets of d-spacings correspond to regions of coexistence. Wavelength of the $P_{\beta'}$ and P_{β} phases is found to be ~ 150 Å and ~ 70 Å, respectively.

	T°C								
RH%	50	45	40	35	30	25	20	15	10
98	55.3	56.8	59.0 ; 63.2	63.9	63.9	63.2 ; 64.7	64.4 ; 66.3	63.9 ; 65.7	63.7 ; 65.7
75	52.1	54.5 ; 59.0	58.8	59.3	59.3 ; 62.4	59.3 ; 62.4	59.0 ; 62.4	59.0 ; 62.5	58.8 ; 62.7

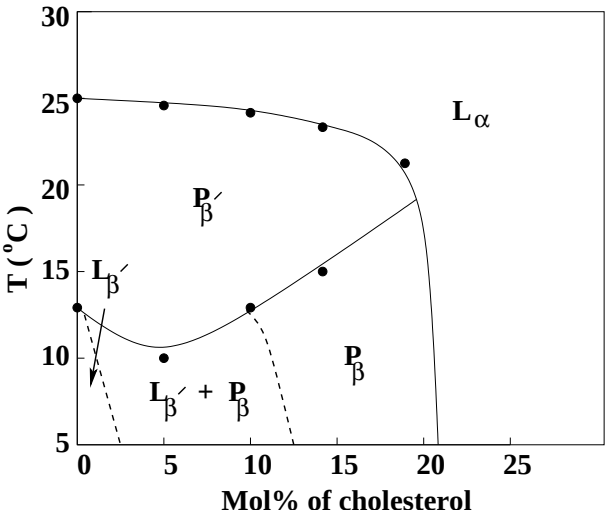

Figure 3.19: Phase diagram of DMPC–cholesterol mixtures at 98% RH, determined from the diffraction data. The phase boundaries indicated by the dotted lines have not been determined very precisely.

corresponding to a larger d-spacing at lower temperatures (Fig. 3.18 b). The phase corresponding to the larger d-spacing might be the P_{β} phase. Although the satellite reflections corresponding to the P_{β} phase at 98% RH were not prominent, we can unambiguously identify this phase at 75% RH from the satellite reflections, as shown in Fig. 3.18 c. At 75% RH, and below T_m we have observed the $P_{\beta'}$ phase throughout the temperature range studied, but satellite reflections at lower temperatures get smeared out, probably due to the increase in wavelength as found in the case of DPPC–cholesterol mixtures. The d-spacings obtained at different temperatures are given in table 3.4.

3.3.4 DMPC–cholesterol

DMPC has the same head group as DPPC, but has two carbon atoms less in each hydrocarbon chain. We have examined the phase behaviour of DMPC–cholesterol mixtures at both 98

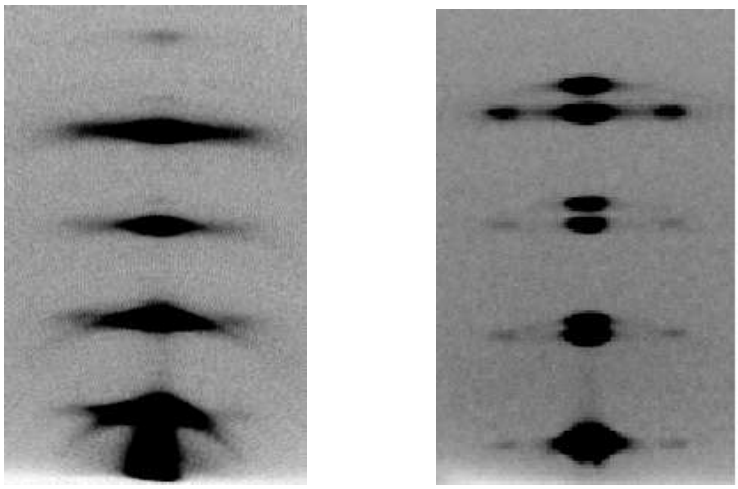

(a) d = 58.8 Å (b) d = 55.1 ; 52.2 (74.5) Å

Figure 3.20: Diffraction patterns of DMPC–cholesterol mixtures. (a) P_β phase (X_c = 15 mol%, T = 5°C, RH = 98%). (b) The coexistence of the P_β and gel phases (X_c = 10 mol%, T = 10°C, RH = 75%). Number in the bracket represents wavelength of the modulation in the P_β phase.

±2% and 75 ±2% RH, in order to check the influence of chain length on the P_β phase.

Phase behaviour of DMPC-cholesterol mixtures was found to be very similar to that of DPPC–cholesterol mixtures (Fig. 3.19). Distinct satellites from the P_β phase was not observed at 98% RH even at 5°C, but this phase could easily be identified from the smearing of the lamellar peaks along $q_\perp$ (Fig. 3.20 a). Good diffraction patterns of this phase was obtained in DPPC-cholesterol mixtures only at temperatures well below the pre-transition. The fact that the pre-transition temperature of DMPC is much lower (~13°C) than that of DPPC (~33°C) might explain the difficulty in obtaining good diffraction patterns of this phase in DMPC–cholesterol mixtures. The coexistence of the P_β and gel phases was observed at intermediate cholesterol concentrations, as in DPPC–cholesterol mixtures. Distinct satellites from the P_β phase were observed in the diffraction pattern at 75% RH (Fig. 3.20 b), when the chain melting transition of the lipid occurs at a much higher temperature [25]. Further, as in DPPC-cholesterol mixtures, this phase is stable over a much larger temperature range at the lower RH.

3.4 Electron density map of the P_β phase

The procedure used to calculate the electron density map has already been discussed in section 2.3.2 of chapter 2. Here we describe the model briefly and present the electron density maps of the P_β and l_o phases obtained from the diffraction data of DPPC–cholesterol mixtures. We have assumed the bilayers in the P_β phase to have a one–dimensional height modulation as in the $P_{\beta'}$ phase, since we have no a priori information about their shape [28]. The rectangular unit cell seen in diffraction patterns of the P_β phase rules out the possibility of thickness modulated bilayers, since packing considerations in such a case can be expected to favour a centered rectangular unit cell. As discussed in chapter 2, a model for the electron density of the bilayers has been used to obtain phases of all the reflections and to calculate the electron density map. The electron density within the unit cell can be described as the convolution of a contour function $C(x,z)$ and a transbilayer profile $T(x,z)$. $C(x,z) = \delta[z - u(x)]$, where $u(x)$ describes the bilayer height profile, which is taken to be triangular. Earlier studies on the ripple phase have shown that an asymmetric bilayer height profile, such as a saw-tooth, would result in an oblique unit cell [29]. The rectangular unit cell seen in the P_β phase, therefore, suggests that the height profile is symmetric, i.e, triangular or sinusoidal. It is also known from earlier studies on the ripple phase that the phases of the reflections obtained from the model are not sensitive to the exact height profile, as long as the symmetry requirements are taken into account. Hence we do not expect the phases to change if a sinusoidal shape is assumed for the height profile instead of the triangular shape.

The transbilayer electron density profile ($T(x,z)$) was modeled using three different models, as discussed in chapter 2. $T(x,z)$ consists of either three delta functions or three Gaussians, two with positive amplitude (ρ_H) corresponding to the head group regions at the surfaces of the bilayer, and one with negative amplitude (ρ_M) corresponding to the methyl group region at the center of the bilayer. In the model with five delta functions, the two additional ones of amplitude ρ_C represent the secondary maxima in the electron density due to cholesterol [20]. Parameters in these models, such as ρ_H, ρ_M, ρ_C, and the bilayer thickness were

obtained by fitting the calculated structure factors with the observed ones. This was done by using standard Levenberg Marquardt technique for nonlinear least squares fitting [30]. Geometric corrections to the diffraction data, relevant to the present experimental geometry, are discussed in chapter 2 [29]. As mentioned in chapter 2, it is difficult to measure the thickness of the sample precisely and, therefore, we have not taken into account absorption corrections to the data. An earlier study on the ripple phase has found that neglecting the absorption correction did not alter the electron density map significantly. This is consistent with the fact that the electron density map is much more sensitive to the phases of the reflections than to their intensities [31].

Table 3.5: Observed structure factor magnitudes ($|\ F_o^{hk}\ |$) of the P_β phase of DPPC–cholesterol mixtures (X_c = 15 mol%, T = 6 °C, RH = 98 ± 2 %) and their best fit values (F_c^{hk}) obtained from the electron density models.

			F_c		
h	k	$\mid F_o \mid$	3 delta	5 delta	3 Gaussian
1	0	10.0	-10.0	-10.0	-10
2	0	7.44	-5.99	-7.67	-4.74
3	0	3.86	3.64	2.73	-1.92
4	0	10.38	-8.59	-9.99	-3.63
5	0	1.27	-1.29	-2.31	0.38
6	0	0.52	0.75	1.30	0.39
7	0	0.53	-2.72	-1.79	-0.40
8	0	0.77	0.07	-0.004	0.10
9	0	1.03	0.09	-0.03	-0.001
2	1	2.79	1.88	2.59	1.26
2	-1	2.79	-1.88	-2.57	-1.26
2	2	-	-0.36	-0.49	-0.20
2	-2	-	-0.36	-0.54	-0.20
3	1	3.25	-1.82	-1.47	-0.79
3	-1	3.25	1.82	1.46	0.79
3	2	-	0.53	0.44	0.19
3	-2	-	0.53	0.46	0.19
4	1	6.43	6.24	7.99	2.14
4	-1	6.43	-6.24	-7.89	-2.14
4	2	1.09	-2.49	-3.35	-0.72
4	-2	1.09	-2.49	-3.45	-0.72
5	2	-	-0.70	-1.54	0.13
5	-2	-	-0.70	-1.53	0.13

Table 3.6: Values of the model parameters obtained from the best fit for DPPC–cholesterol mixtures in the P_β and l_o phases. A is the amplitude of the height modulation in the P_β phase. x_h and x_c are the distances of the peaks corresponding to the headgroup and cholesterol from the center of the bilayer, respectively. σ_h and σ_m are the widths of the Gaussians corresponding to the head group and the terminal methyl group, respectively, in the three Gaussian model. Σ is the function to be minimized in the fitting routine.

X_c (mol%		A	x_h	x_c	$\frac{2\rho_H}{\rho_M}$	$\frac{2\rho_C}{\rho_M}$	σ_h	σ_m	Σ
15 (P_β)	3 delta	7.9	23.6	-	2.25	-	-	-	23.0
	5 delta	8.3	23.3	9.4	2.16	0.38	-	-	33
	3 Gaussian	6.7	23.9	-	2.0	-	2.9	4.9	113
50 (l_o)	5 delta	-	20.3	11.0	1.6	0.4	-	-	494
	3 Gaussian	-	19.89	-	1.58	-	1.93	5.97	8.0

The five delta function model does not give a better fit than the three delta function model for $T(x, z)$. However, the phases obtained from these two models are the same for all strong reflections but phases of a few weak reflections do change with the model. For a given model phases of some weak reflections are also found to change with the starting values of the material parameters in the model. The converged values of the model parameters are sensitive to the initial values of these parameters. For some initial values, we obtain unrealistic final values of the model parameters. This could be due to the presence of multiple local minima of the function Σ (defined in chapter 2) in the parameter space. We also used a model, where the three delta functions were replaced with Gaussians. But a model with five Gaussians could not be used, since the model parameters did not converge, probably due to the large number of parameters in it. Although we would expect a Gaussian to represent the head group and terminal methyl regions better than three delta function, the model gives a poorer fit. The reason for this discrepancy is presently not clear. Structure factors obtained from the fit using the three models and the observed ones are given in table 3.5. Converged values of the model parameters are given in table 3.6. The calculated phases were combined with the observed magnitudes, and inverse Fourier transformed to get the two-dimensional electron density map, shown in Fig. 3.21. It clearly shows a stack of modulated bilayers separated by water. The quality of the map is very good, indicating that the model used to

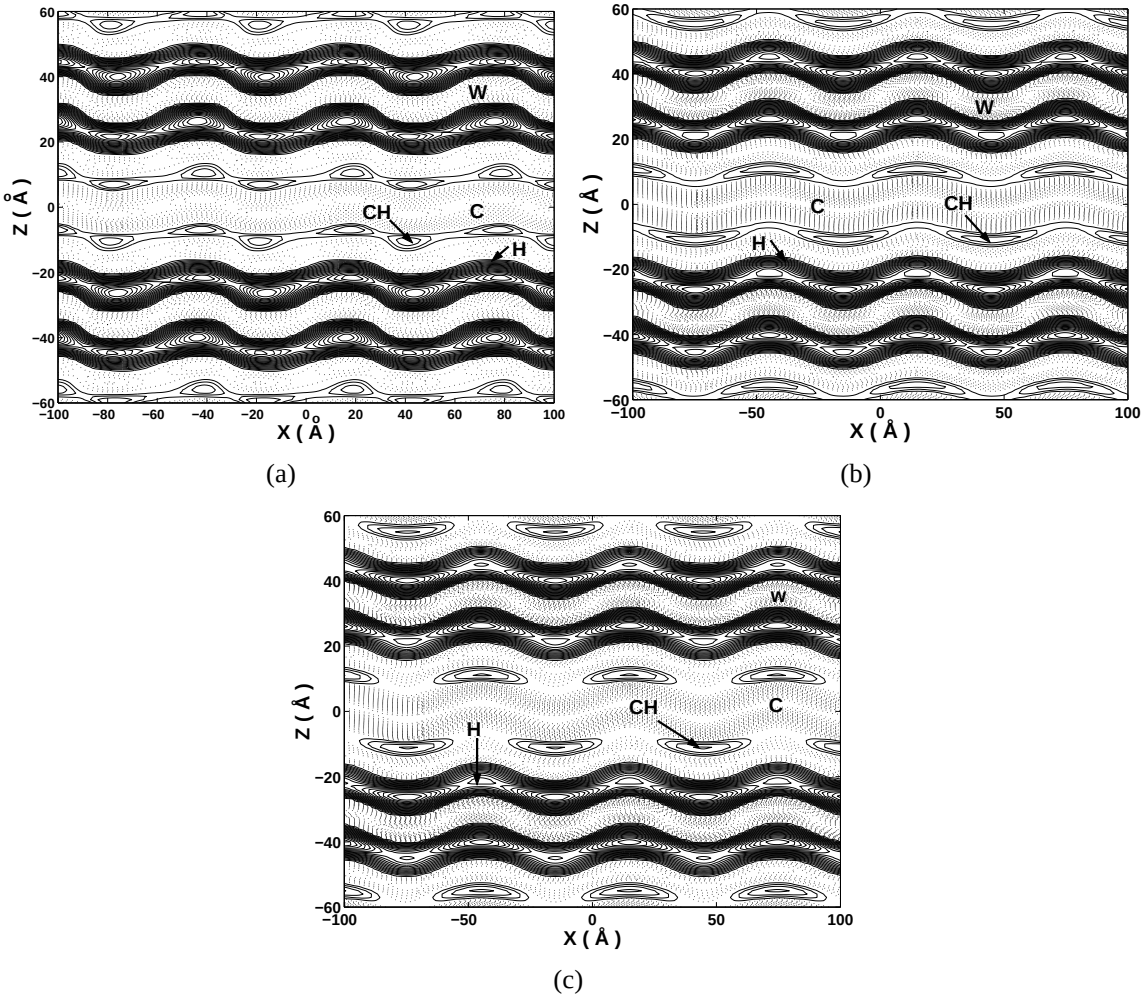

Figure 3.21: Electron density map of the P_β phase of DPPC–cholesterol mixtures calculated from the diffraction data of table 3.5, using the phases obtained with the three delta function (a), five delta function (b) and three Gaussian (c) models. The solid (dotted) contours correspond to the electron rich (poor) regions of the bilayers. H, W and C denote the head group, water and chain regions of the bilayer, respectively. CH denotes the electron rich band in the bilayer due to the presence of cholesterol. X_c = 15 mol%, T = 6°C, RH = 98 %, d = 66.3 Å, λ = 60.7 Å.

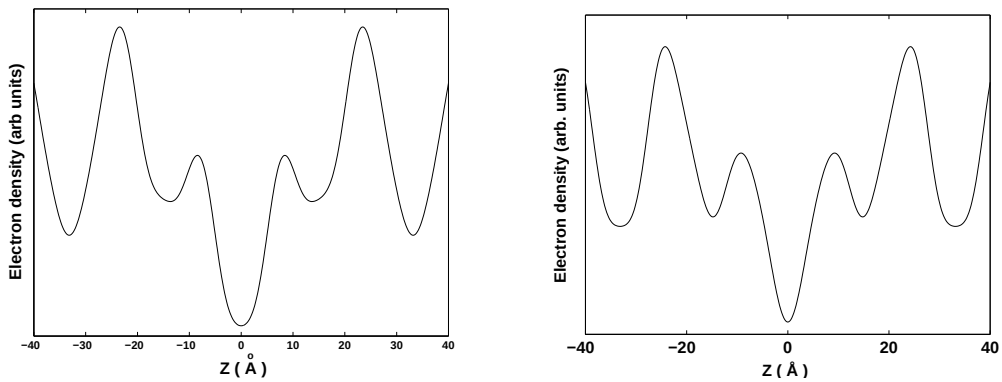

(a) (b)

Figure 3.22: The transbilayer electron density profiles at $x = 0$ obtained from the electron density maps shown in Fig. 3.21. using three delta function (a) and five delta function (b) models. Peaks near ± 22 Å and the trough at the center correspond to the head group regions and the terminal methyl groups of hydrocarbon chains, respectively. The secondary maxima near ± 10 Å are due to the presence of cholesterol in the bilayers.

phase the reflections is essentially correct. The height modulations of the bilayers obtained from the three delta function model are slightly asymmetric (arms of unequal length), as shown in Fig. 3.21 a. However, the maps obtained from the five delta function and the three Gaussian models seem to have more symmetric height profiles (Fig. 3.21 b and c) as expected from the diffraction pattern. The transbilayer profiles obtained from the maps (Fig. 3.21) at $x = 0$ using three and five delta function models are shown in Fig. 3.22 a and b, respectively.

We have also constructed one dimensional transbilayer electron density profile of the l_o phase using the five delta function and the three Gaussian models (Fig. 3.23). Phases obtained from these two models are essentially the same, but the Gaussian model gives a better fit with the experimental data, compared to the five delta function model. The phases of some weak reflections do change with different starting values of the material parameters. However, the phases of these weak reflection do not affect the electron density map significantly. The fit from the three delta function is very poor and the phases obtained from this model could not be used to calculate the electron density map. The observed and calculated structure factors from the five delta function and three Gaussian models are given in table 3.7.

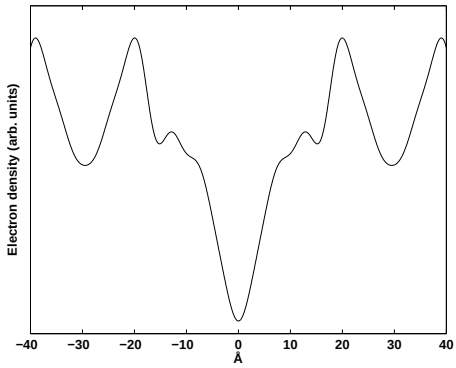

Figure 3.23: Transbilayer electron density profile in the l_o phase of DPPC at 50 mol% of cholesterol (T = 24°C, Rh =98%), calculated from the data given in table 3.7. Peaks near ± 20 Å and the trough at the center correspond to the head groups and terminal methyl groups of hydrocarbon chains, respectively. Peaks near ± 10 Å are due to the presence of cholesterol.

Table 3.7: Observed structure factors (| F_o^{hk} |) of the l_o phase of DPPC–cholesterol mixture (X_c = 50 mol%, T = 24°C) and their best fit values (F_c^{hk}) obtained from the five delta function and the three Gaussian models.

		F_c	
h	| F_o |	3 Gaussian	5 delta
1	10.00	-10.00	-10.00
2	7.72	-6.96	-11.15
3	0.78	1.20	0.94
4	5.16	-2.80	-12.30
5	0.71	-1.31	-5.32
6	0.82	2.03	4.44
7	1.14	-1.03	-14.49
8	0.54	-0.38	-8.30
9	0.95	0.79	1.00
10	-	-0.37	-12.5
11	0.55	-0.09	-1.81
12	-	0.20	0.63

3.5 Discussion

The results presented here show that the modulated (P_β) phase differs in many ways from the ripple ($P_{\beta'}$) phase. First of all, $P_{\beta'}$ is well known to occur only at very high RH, close to 100 %. In contrast, P_β occurs even at 75 % RH. Secondly, the variation of the modulation wavelength (λ) with cholesterol content shows opposite trends in the two phases. In the $P_{\beta'}$ phase λ increases with X_c and seems to diverge near $X_c \sim 20$ mol% (Fig. 3.5) [21]. On the other hand, in the P_β phase it decreases with X_c and tends to zero at a similar concentration (Fig. 3.13). The temperature dependence of λ in the P_β phase has also been found to be opposite to that of $P_{\beta'}$ phase [19]. λ at a given X_c decreases with increasing temperatures in the $P_{\beta'}$ phase, whereas the P_β phase shows the opposite trend as shown in Fig. 3.13.

The electron density map (Fig. 3.21) suggests that these bilayers have a rather small height modulation, with an amplitude of ~ 2.5 Å, which is about 5 times smaller than that seen typically in the $P_{\beta'}$ phase. An electron rich band is clearly seen in Fig. 3.21 at a distance of about 10 Å from the bilayer center, in addition to the one corresponding to the head group region. Its position is very close to that of a secondary peak due to cholesterol seen in the electron density profiles of DPPC–cholesterol bilayers [20]. The bilayer thickness is also in good agreement with earlier reports [20]. These maps also suggest that the cholesterol concentration within the bilayer alternates periodically between the two monolayers making up a bilayer. Such a distribution of cholesterol would make the bilayer locally asymmetric and can in principle lead to a local curvature of the bilayer. This can explain the observed small amplitude periodic height modulation of the bilayer. However, as we have diffraction data over a very limited q-range, we cannot presently rule out the possibility that this short length scale modulations in the cholesterol concentration is an artifact of the Fourier reconstruction of the electron density.

The oblique unit cell of the $P_{\beta'}$ phase is a consequence of different bilayer thicknesses in the two arms of the ripple, which can at least partly be accounted for by a chain tilt along the ripple wave vector [32]. On the other hand, there is no evidence for a chain tilt along this

direction in the P_β phase, and the bilayer thickness in the two arms are comparable.

If the basic structural feature of the P_β phase is an in-plane modulation in the cholesterol concentration, instead of a height modulation as assumed in the electron density model, one would expect the (0, k) reflections to be very prominent, since they correspond to variations in the electron density, projected on to the plane of the bilayer. We have carried out experiments to check this possibility, by aligning the bilayers normal to the x-ray beam. Although we were able to observe a diffuse wide angle peak from the chains, no peaks were seen in the small angle region corresponding to the (0, k) reflections. This result rules out a structure similar to that of a stripe phase with strong in-plane modulation of cholesterol concentration. On the other hand, this observation is consistent with the structure inferred from the electron density map, since the intensity of the (0,1) reflection calculated from the model for the values of the parameter obtained from the fit is a few orders of magnitude smaller than that of the (1,0) reflection.

The P_β phase reported here has not been seen in earlier freeze fracture, spectroscopic and diffraction studies of lipid–cholesterol membranes [7, 9, 18, 19, 21]. One possible reason for not resolving this structure in freeze fracture studies could be the very low amplitude of the ripples. Since platinum deposition is usually done at an angle of 45°, such low amplitude ripples will not lead to a shadowing effect. As spectroscopic studies, such as NMR, probe the local structure of the bilayer, we would not expect them to reveal the modulated feature in the P_β phase, although this phase was identified as a cholesterol–rich β phase [26]. Most of the x-ray and neutron scattering studies have been carried out on unoriented samples. This could lead to the overlapping of satellite reflections with the lamellar reflections in the diffraction pattern, and make the identification of the modulated phase difficult. As can be seen from our unoriented diffraction data of DPPC–cholesterol mixtures, the lamellar phase at $5 \leq X_c \leq 10$ can swell giving rise to a large d-spacing of $\sim$ 85 Å. This is the range of X_c in which the P_β phase occurs. We have not observed the coexistence of the P_β with the gel phase in these unoriented sample. However, the coexistence of two lamellar phases has been reported in this system over a range of cholesterol concentration, similar to that over which

the gel-P_β coexistence is seen in the present study [18]. The relatively large lamellar periodicity of the cholesterol–rich phase coexisting with the $L_{\beta'}$ phase for $3 < X_c < 10$, reported in ref. [18], clearly shows that the bilayers in this phase are rather flexible. This is again supported by the fact that a few lamellar reflections were observed and the higher order lamellar reflections are broad. The occurrence of the modulated phase, which has not been seen in other lipid systems, might also be a consequence of the enhanced bilayer flexibility due to the presence of cholesterol in this phase. It is possible that on swelling the height modulation of the bilayers are no more correlated. Therefore, the P_β phase might not exist with excess water. In ref. [18] it was suggested that this increase in d might be the consequence of a decrease in the attractive van der Waals interaction between the bilayers on incorporating cholesterol. However, the fact that the l_o phase with much higher X_c has a smaller d does not support this conjecture. Therefore, it is likely that this increase in d arises from an increase in the steric repulsion between the bilayers, resulting from thermal undulations of the bilayers [33]. Indeed some recent studies have indicated a softening of the bilayers at comparable cholesterol concentrations [34], which can account for the enhanced thermal undulations. Our fluorescence microscopy studies on giant unilamellar vesicles made up of these mixtures show significant thermal shape fluctuations at small values of X_c, revealing an unexpected softening of the bilayers. Microscopy observation will be discussed in detail in chapter 7. At high cholesterol content ($X_c > 30$), bilayers are more rigid and no swelling behaviour was observed with temperature. The d-spacing becomes comparable with that of the L_α phase of the pure lipid, as shown in table 3.2.

The condensed wide angle reflection in the l_o phase shows that the hydrocarbon chains of the lipid molecules are stretched by the intercalated cholesterol molecules. The presence of a larger number of lamellar reflections in this phase can be understood in terms of the higher rigidity of the bilayers in the presence of cholesterol [35]. The intensity profiles of the wide angle chain reflections of DPPC at T = 24 °C for a few cholesterol concentrations are plotted in Fig. 3.24 . The two reflections in the $L_{\beta'}$ phase of DPPC result from a chain tilt towards nearest neighbour [24]. The on-axis reflection is much weaker because of absorption by the

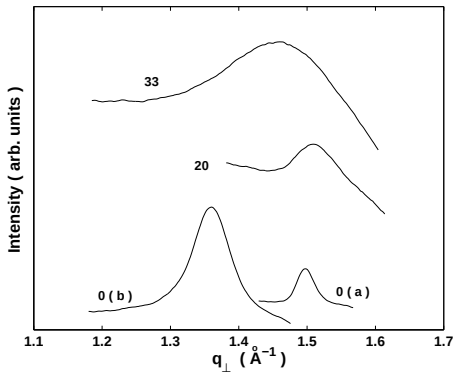

Figure 3.24: Profiles of the wide angle chain reflection in the different phases exhibited by the DPPC–cholesterol mixtures. The numbers against the curves indicate X_c. (a) and (b) refer to the on-axis ($q_z = 0$) and off-axis reflections in the $L_{\beta'}$ phase of DPPC, respectively. $X_c = 20$ mol% corresponds to the P_β phase, and $X_c = 33$ mol% to the L_α phase.

substrate. The width of these reflections is inversely proportional to the correlation length, ξ, of the chain ordering in the plane of bilayer. The wide angle peak is initially sharp in the gel phase, but gets gradually broader as the cholesterol content is increased, indicating that the correlation length of chain ordering decreases gradually with X_c at temperatures below the chain melting transition of the pure lipid. The width is not very different in the P_β phase, indicating a high degree of in-plane order. As to be expected, the width is much larger in the fluid L_α phase. However, the width of the chain reflection along q_z in the cholesterol–rich L_α phase is not very large (Fig. 3.10), due to the stretching of the chains in the presence of cholesterol (Fig. 3.25) [20].

It is interesting to note that modulated bilayers similar to those in the P_β phase have been predicted by a Landau theory of phase transitions in bilayers [36]. In an achiral system, only symmetric ripples are possible, whereas in chiral system both symmetric and asymmetric ripple are predicted. The asymmetric ripples have a chain tilt normal to the ripple wave vector ($\vec{q}$), which is oscillatory along $\vec{q}$. We cannot conclusively rule out such tilt oscillations in the P_β phase if they are of small amplitude. On the other hand the symmetric ripples have a mean tilt normal to $\vec{q}$. The system studied by us are chiral and either of these phases is, therefore, possible. However, since we are not able to infer the detailed chain packing from the electron density map, we cannot confirm either of these structures from our present data.

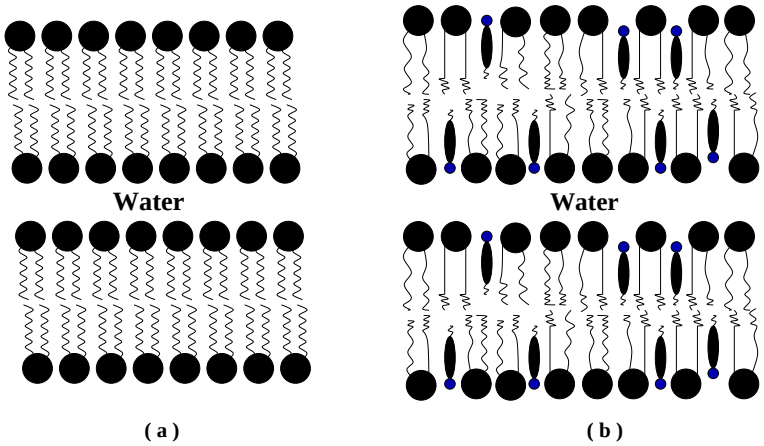

Figure 3.25: Schematic diagram of bilayers showing the fluid (L_α) phase in the absence of cholesterol (a). For comparison, (b) the fluid (L_α) phase in the presence of cholesterol is also shown. Stretching of hydrocarbon chains of the lipids in the presence of cholesterol is depicted in (b).

The similarity of the phase behaviour found in DMPC–cholesterol mixtures to that of DPPC–cholesterol mixtures is not surprising since the phase behaviour of the two lipids themselves are very similar. As the T_m of DMPC is lower and the length of the hydrocarbon chains shorter, the temperature range of different phases and their d-spacings are expected to be different from that of DPPC–cholesterol mixtures.

The binary PC–cholesterol mixtures do not exhibit fluid–fluid immiscibility above the chain melting transition temperature (T_m) in any of the diffraction studies. However, spectroscopic technique, such as NMR, has revealed such a coexistence. It is clear that the gel phase is immiscible with the cholesterol–rich P_β phase at lower temperatures and the cholesterol content in the gel phase is negligible. Further, the cholesterol distribution in the P_β phase may also be nonuniform as revealed from the electron density map (Fig. 3.21). On increasing the temperature, the cholesterol–rich phase might break up into small microscopic domains, whereas the gel phase is transformed into the fluid (L_α) phase. These cholesterol–rich domains must have different chain conformational order, as the presence of cholesterol leads to the stretching of the lipid chains (Fig. 3.25), resulting in a more ordered fluid state, compared to the cholesterol–poor region of the membrane. Therefore, above T_m, we could still have the coexistence of two phases with different chain conformational order of the lipid

which can easily be detected using NMR. However, the small angle x-ray diffraction technique cannot detect these microscopic domains since there is negligible contrast between the two phases. This explains the difficulty in detecting the coexistence of the two fluid phases above T_m using diffraction studies.

The form factor corresponding to the ripple profile in the P_β phase depends on the angle between two arms of the bilayers . For small angles, it is spread out over a larger $q_\perp$ range. However, as the angle becomes larger, intensity of the reflections at larger $q_\perp$ becomes negligible. Therefore, the fact that higher order satellite reflections were not observed for larger X_c, indicates an increase in the angle between the two arms of the bilayers. As mentioned earlier, the wavelength of the modulation decreases with increasing X_c (Fig. 3.13). These two observations taken together require the amplitude of the modulation to decrease with increasing X_c. Therefore, both the amplitude and wavelength tend to zero at sufficiently large values of X_c (>22 mol%), leading to a l_o phase where the cholesterol distribution in the bilayer is almost uniform. The fact that we have not observed the coexistence of the P_β and l_o phases suggests that the transition from the P_β to the l_o phase is continuous.

It is interesting to note that the cholesterol analog DHE also stabilizes the modulated phase at lower temperatures (below T_p). In addition, P_β phase was found to coexist with the $P_{\beta'}$ phase at lower temperatures, both at 98% and 75% RH. Occurrence of the $P_{\beta'}$ phase at low RH is intriguing. The ripple wavelength ($\lambda \sim 150$ Å) of the $P_{\beta'}$ phase is similar to that observed in the case of the pure lipid, whereas the wavelength of the P_β phase is ~ 70 Å. However, the oblique angle (γ) of the $P_{\beta'}$ phase reduces from more than 90° to $\sim 90°$ as the temperature is decreased. Therefore, it is evident that small change in the sterol structure can lead to observable differences in the phase behaviour.

The formation of the P_β phase at intermediate X_c is rather intriguing. We suspect that the miscibility gap between the $L_{\beta'}$ and P_β phases is a consequence of the non-zero tilt in the former. As is well known, the chain tilt arises from the larger cross-sectional area of the head group compared to that of the chains. Therefore, if the tilt can take only values close to 30 and 0° (as observed experimentally), it is conceivable that a well-defined amount of choles-

terol has to be incorporated into the bilayer to remove the tilt. A rough estimate based on the areas of the different moieties gives $X_c \approx 20$ mol% in the untilted phase. Therefore, for $X_c <$ 20 mol%, the cholesterol distribution in the bilayer can be nonuniform with cholesterol free regions alternating with regions where $X_c \approx 20$ mol%. Such a nonuniform distribution of cholesterol is seen in the electron density map (Fig. 3.21), where the distribution of cholesterol alternates between the two monolayers making the bilayer locally asymmetric. Such an asymmetry can lead to a non-zero local spontaneous curvature of the bilayers. Therefore, the height modulation in the P_β phase might be the consequence of local spontaneous curvature due to the out of phase periodic localization of cholesterol in the two monolayers making up a bilayer.

3.6 Conclusion

We have systematically studied the phase behaviour of mixtures of cholesterol with DPPC and DMPC. A modulated (P_β) phase is found in PC-cholesterol mixtures at intermediate cholesterol concentrations, whose structure is somewhat similar to that of the ripple phase seen in some PCs in between the main- and pre-transitions. These two phases, however, differ in the dependence of their structural parameters on cholesterol concentration and on relative humidity. The electron density map of the P_β phase calculated from the observed diffraction pattern shows a periodic height modulation of bilayers of amplitude ~ 2.5 Å. The length and the bilayer thickness of the two arms of the ripple are found to be similar, unlike in the $P_{\beta'}$ phase. At higher cholesterol concentrations these binary systems exhibit a fluid lamellar phase, with a higher degree of chain ordering compared to the L_α phase of the pure lipids.

Bibliography

[1] L. Finegold, ed. *Cholesterol in Membrane Models* (CRC Press, Boca Raton, FL, 1993).

[2] M. Edidin, Annu. Rev. Biophys. Biomol. Struct. **32**, 257 (2003).

[3] D. A. Brown and E. London, J. Biol. Chem. **275**, 17221 (2000).

[4] C. Dietrich, L. A. Bagatolli, Z. N. Volovyk, N. L. Thompson, M. Levi, K. Jacobson, and E. Gratton, Biophys. J. **80**, 1417 (2001).

[5] J. R. Silvius, Biochim. Biophys. Acta **1610**, 174 (2003).

[6] W. Knoll, G. Schmidt, K. Ibel, and E. Sackmann, Biochemistry **24**, 5240 (1985).

[7] M. R. Vist and J. H. Davis, Biochemistry **29**, 451 (1990).

[8] M. B. Sankaram and T. E. Thompson, Biochemistry **29**, 10670 (1990).

[9] B. R. Lentz, D. A. Barrow, and M. Hoechli, Biochemistry **19**, 1943 (1980).

[10] C. Paré and M. Lafleur, Biophys. J. **74**, 899 (1998).

[11] T. P. W. McMullen, R. N. A. H. Lewis, and R. N. McElhaney, Biochim. Biophys. Acta **1416**, 119 (1999).

[12] T. P. W. McMullen, R. N. A. H. Lewis, and R. N. McElhaney, Biochemistry **32**, 516 (1993).

[13] S. W. Hui and N. B. He, Biochemistry **22**, 1159 (1983).

[14] M. B. Sankaram and T. E. Thompson, Proc. Natl. Acad. Sci. U.S.A. **88**, 8686 (1991).

[15] Y. Kim, R. Tero, M. Takizawa, and T. Urisu, Japanese J. Appl. Phys. **43**, 3860 (2004).

[16] J. H. Ipsen, G. Karlström, O. G. Mouritsen, H. Wennerström , and M. J. Zuckermann, Biochim. Biophys. Acta **905**, 162 (1987).

[17] A. Filippov, G. Orädd, and G. Lindblom, Biophys. J. **84**, 3079 (2003).

[18] R. P. Rand, V. A. Parsegian, J. A. C. Henry, L. J. Lis, and M. McAlister, Can. J. Biochem. **58**, 959 (1980).

[19] K. Mortensen, W. Pfeiffer, E. Sackmann, and W. Knoll, Biochim. Biophys. Acta **945**, 221 (1988).

[20] T. J. McIntosh, Biochim. Biophys. Acta **513**, 43 (1978).

[21] B. R. Copeland and H. M. McConnell, Biochim. Biophys. Acta **599**, 95 (1980).

[22] F. Richter, G. Rapp, and L. Finegold, Phys. Rev. E **63**, 051914 (2001).

[23] M. J. Janiak, D. M Small, and G. G. Shipley, Biochemistry **15**, 4575 (1976).

[24] M. Hentschel and R. Hosemann, Mol. Cryst. Liq. Cryst. **94**, 291 (1983).

[25] G. S. Smith, E. B. Sirota, C. R. Safinya, R. J. Plano, and N. A. Clark, J. Chem. Phys. **92**, 4519 (1990).

[26] D. Bach and E. Wachtel, Biochim. Biophys. Acta **1610**, 187 (2003).

[27] E. London and D. A. Brown, Biochim. Biophys. Acta **1508**, 182 (2000).

[28] W. -J. Sun, S. Tristram-Nagle, R. M. Suter, and J. F. Nagle, Proc. Natl. Acad. Sci. U.S.A. **93**, 7008 (1996).

[29] K. Sengupta, V. A. Raghunathan, and J. Katsaras, Phys. Rev. E **68**, 031710 (2003).

[30] W. H. Press, S. A. Teukolsky, W. T. Vetterling, and B. P. Flannery, *Numerical Recipes* (Cambridge University Press, 1992).

[31] G. N. Ramachandran and R. Srinivasan, *Fourier Methods in Crystallography* (Wiley Interscience, New York, 1970).

[32] K. Sengupta, V. A. Raghunathan, and Y. Hatwalne, Phys. Rev. Lett. **87**, 055705 (2001).

[33] W. Helfrich, Z. Naturforsch. **28**c, 693 (1973).

[34] M. Rappolt, M. F. Vidal, M. Kriechbaum, M. Steinhart, H. Amenitsch, S. Bernstorff, and P. Laggner, Eur. Biophys. J. **31**, 575 (2003).

[35] P. Méléard, C. Gerbeaud, T. Pott, L. Fernandez-Puente, I. Bivas, M. D. Mitov, J. Dufourcq, and P. Bothorel, Biophys. J. **72**, 2616 (1997).

[36] T. C. Lubensky and F. C. MacKintosh, Phys. Rev. Lett. **71**, 1565 (1993); C.-M. Chen, T. C. Lubensky, and F. C. MacKintosh, Phys. Rev. E **51**, 504 (1995).